Chapter 1

An overview of Energy, its diverse origins, and significant challenges linked to its storage and conversion

In this chapter, we will provide a brief overview of energy and explore different types of energy sources, that includes renewable and non-renewable sources. Our focus is on the future outlook of global energy and finding the most suitable alternatives to fossil fuels, taking into concerns such as global warming and climate change, which arise due to the net carbon addition to the earth's atmosphere. Additionally, we provide a concise overview of electrochemical energy storage (EES) systems, categorizing them based on their charge storage principles, and compiling various phenomena associated with them. The final section of this chapter concludes by highlighting different types of electrode materials, more particularly, redox-mediated intercalative pseudocapacitor electrodes, that offer solutions for grid-level energy storage technology in the future.

1.1 An Introduction to Energy

Energy is a fundamental property of matter and space that plays a pivotal role in every aspect of our lives. From the moment we wake up and interact with our environment to global industrialization, energy is the core of all activities. From the beginning of the formation of our planet Earth, energy exchange plays a crucial role in making our planet inhabitable and hence can be considered as the "basis of existence" [1][2]. Just a few million years ago, our own species, Homo sapiens, first appeared, then strived most of history, and boomed with agriculture and the Industrial Revolution. Across the ages, humans have acquired knowledge on harnessing and utilizing energy in various forms to accomplish productive work, defining energy as the ability of a system to perform work. However, due to its multiple existences, it is quite difficult to find out one comprehensive definition of energy. Consequently, it is considered as the property of materials that can be transferred to each other but cannot be created or destroyed. This concept leads to the foundation of the fundamental law of physics, known as the conservation of energy.

Standards of living and energy use have been growing exponentially and in the coming future two things are certain: (1) the world population will increase exponentially and (2) economic reserves of fossil fuels, particularly oil, coal, and natural gas, will decrease substantially [3]. So, in the next several decades, the world will face global energy problems and environmental concerns such as global warming and climate change. New technology and better living habits must be developed to fulfill the ever-increasing energy needs and to preserve the quality of our environment.

The world population is about 6.3 billion, with total energy consumption of about 2.21 kW per capita. The total energy coming to the Earth's surface is 99.98% solar, 0.02% geothermal, and 0.02% tidal/gravitational. Currently, about 14 TW (or 2.21 kW per capita) of the world's energy consumption rate represents only a tiny fraction-0.008% of the solar energy striking to the Earth, which is six times smaller than the total global photosynthesis process [4]–[6]. However, most of the solar energy coming to the Earth's surface is time, location, and weather-dependent and cannot be used directly in electrical and electronic

appliances. Other issues related to renewable energy plants are they are quite smaller compared to traditional power plants for electricity generation, thus renewable energy will need access to the electrical grid to transport the electricity to the consumers. Therefore, energy storage and conversion efficiencies become a key challenge to harnessing the full potential of renewable energy sources, and thus grid-scale energy storage solutions are needed to reduce the burden of fossil-fuel-based energy solutions.

1.2 Different types of Energy sources

There are mainly two categories of energy sources available in the world: Non-renewable and Renewable energy sources.

1.2.1 Non-renewable energy sources

Non-renewable energy sources are finite resources that cannot be naturally replenished within a short timeframe. These sources were formed over millions of years and are being consumed at a much faster rate than they are being replenished. Furthermore, extracting of energy from non-renewable energy sources produces carbon dioxide (CO_2) and other greenhouse gases into the atmosphere, contributing to climate change and air pollution [7]. As a result, many countries are transitioning from coal to renewable energy alternatives like solar, wind, and hydroelectric power. Here are some examples of non-renewable energy sources:

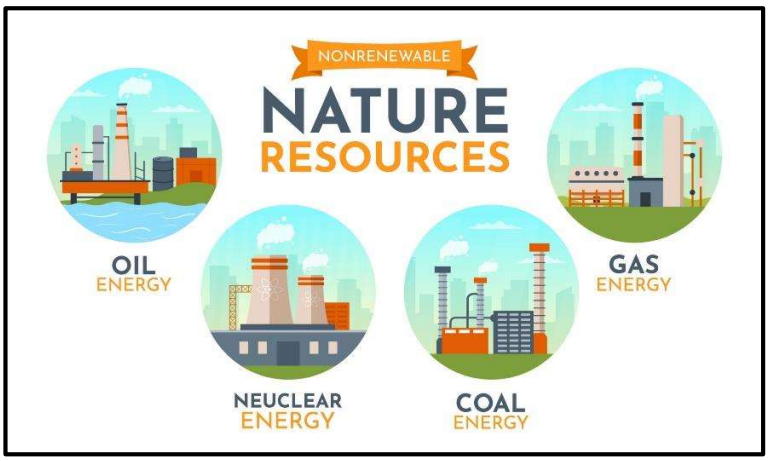

Figure 1.1: Different types of non-renewable energy sources [open access internet source]

1.2.2 Renewable energy sources

Renewable energy sources are those that can be replenished naturally within a relatively short period of time. They are considered sustainable because their availability is virtually limitless and they have a minimal impact on the environment. It is a clean energy source, as it produces no greenhouse gas emissions or air pollutants during operation. It helps in reducing reliance on fossil fuels and mitigates the negative impacts associated with their extraction and combustion. Here are some examples of renewable energy sources that include solar energy, wind energy, geothermal energy, hydropower, biomass, and tidal energy, which have been considered as a more sustainable future energy source [8]–[10].

Table 1.1: Different type of non-renewable and renewable energy source and its applications [10]

Types	Source	Energy conversion and application
Non-Renewable	**Coal**	Heat generation, Electricity generation, powering industry
	Oil	Production of gasoline, diesel fuel, and petroleum
	Natural gas	Electricity generation, heating, cooking, and industrial process
	Nuclear	Nuclear fission, Nuclear fusion, Continuous power supply
Renewable	**Solar energy**	Solar panels, Photovoltaic, thermal power generation
	Wind energy	Power generation, wind generators, water pump
	Hydropower	Power generation from flowing water
	Geothermal	Urban heating, hot rocks or magma, hydrothermal
	Biomass	Pyrolysis, gasification, digestion, heat power generation

Figure 1.2: Different types renewable energy sources [open access internet source]

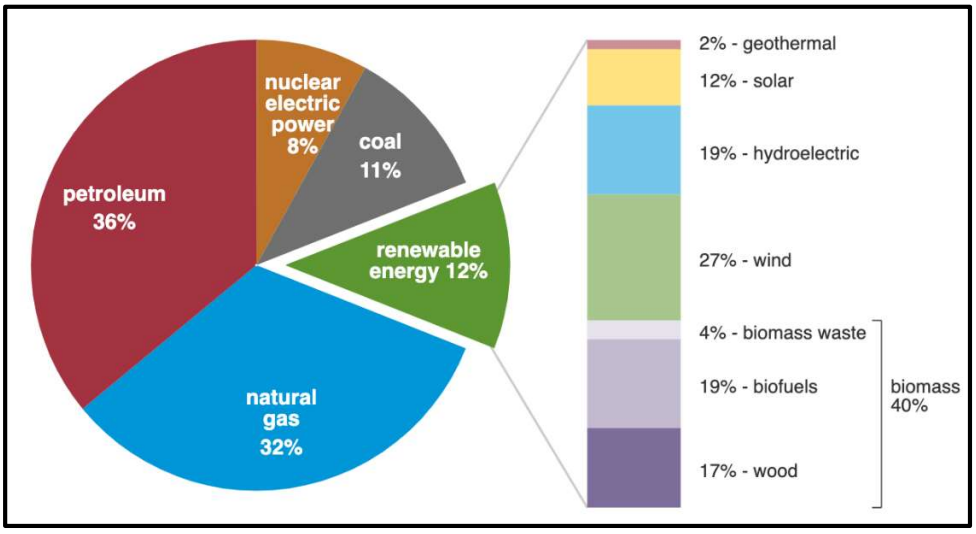

Figure 1.3: Worldwide consumption rate of different types energy sources [11][12].

1.3 Requirement of Renewable energy sources and its challenge

One of the key objectives of utilizing renewable energy sources is to decrease reliance on fossil fuels and mitigate environmental concerns like global warming and climate change [11][12]. Technologies like solar, wind, hydro, and geothermal offer cleaner alternatives that substantially decrease the emission of greenhouse gases and air pollution. To tackle climate change effectively, it is crucial that renewable energy technologies operate with minimal or zero carbon dioxide (CO_2) emissions. Another requirement is to enhance energy security and decrease dependency on foreign energy sources. Renewable energy can be generated locally, utilizing abundant domestic resources, thereby reducing vulnerability to geopolitical tensions and price fluctuations linked to the importation of fossil fuels. Consequently, renewable energy sources provide a sustainable and resilient energy future that can effectively reduce greenhouse gas emissions, mitigate climate change, and ensure a reliable and cost-effective energy supply for the world.

Despite significant advantages, several renewable energy technologies are still in the early stages of development. The availability of renewable energy sources is intermittent and subject to variations in time and weather conditions. Solar power relies on sunlight, while wind power depends on wind speeds. This intermittent nature creates difficulties in maintaining grid stability and necessitates the implementation of energy storage solutions and smart grid technologies to manage the fluctuating supply and demand [13]. Grids designed for centralized power generation from fossil fuels must adapt to accommodate distributed and decentralized renewable energy sources. Upgrading and expanding transmission and distribution infrastructure to connect renewable energy generation sites to population centers can also pose logistical and financial challenges. Conclusively, it is essential to develop smart energy storage solutions to ensure the balance between the demand and supply of energy at all times and everywhere [14]. These challenges require ongoing research and development, technological advancements, supportive policies, and international collaboration to expedite the transition toward a sustainable energy future.

1.4 Renewable Energy storage solutions

Renewable energy storage solutions are technologies designed to store energy generated from renewable sources such as solar, wind, hydro, and geothermal power. These storage solutions help balance the supply and demand of renewable energy, enable grid stabilization, and enhance the integration of renewable sources into existing power systems. Several energy storage solutions already exist in the market and are commonly implemented on a daily basis. Some of them are given as following:

(1) Mechanical [15] **(2)** Thermal ES [16] **(3)** SMES [17] **(4)** Hydrogen [18] **(5)** Electrochemical Energy storage [19].

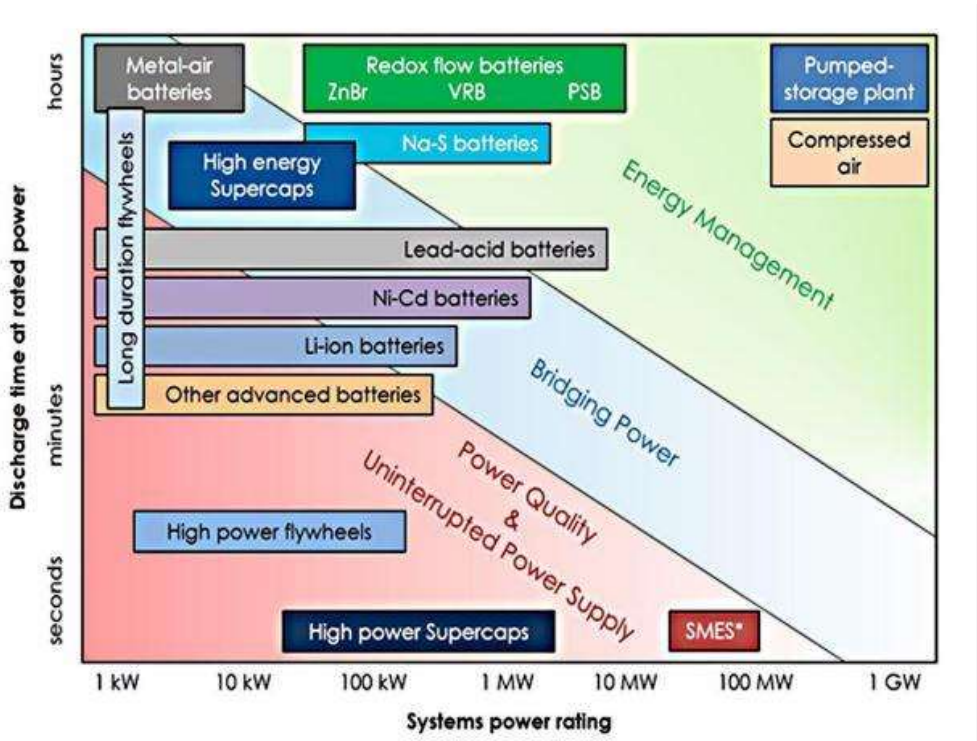

Figure 1.4: Suitability of energy storage technologies to different power and rate of discharge requirements (source: Sandia National Laboratories) [20].

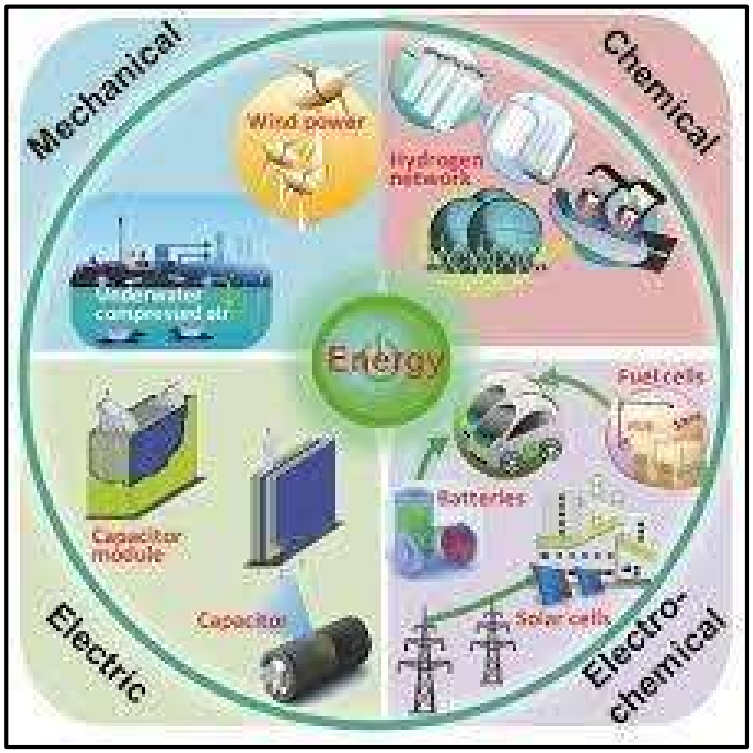

Figure 1.5: Different types of grid energy storage technologies [21].

1.5 Electrochemical Energy Storage Systems (EES)

Electrochemical energy storage devices are getting much attention in recent years due to their higher conversion efficiency and fast power delivery capabilities. These devices store energy through chemical reactions and convert it into electrical energy when required. The increasing demand for portable power sources in mobile devices, electric vehicles, and the Internet of Things has compelled researchers to develop efficient EES [22]–[25]. Essentially, all these devices involve the movement of ions between two electrodes, accompanied by the flow of electrons in an external circuit [26][27]. Ideally, an EES device should possess the ability to store large amount of energy (i.e., high specific energy) and be capable of rapid charging and discharging (i.e., high specific power), as depicted in a graph called a Ragone plot [25][28] (Fig. 1.6), which shows the relationship between energy density (Wh/kg) and power density (W/kg) of various devices. Among various EES devices, as shown in Fig. 1.6, fuel cells possess ultrahigh energy density but suffer from slow kinetics (low power density)

and need expensive catalysts. As for capacitors, the ultralow energy density limits their application in fast power supplies.

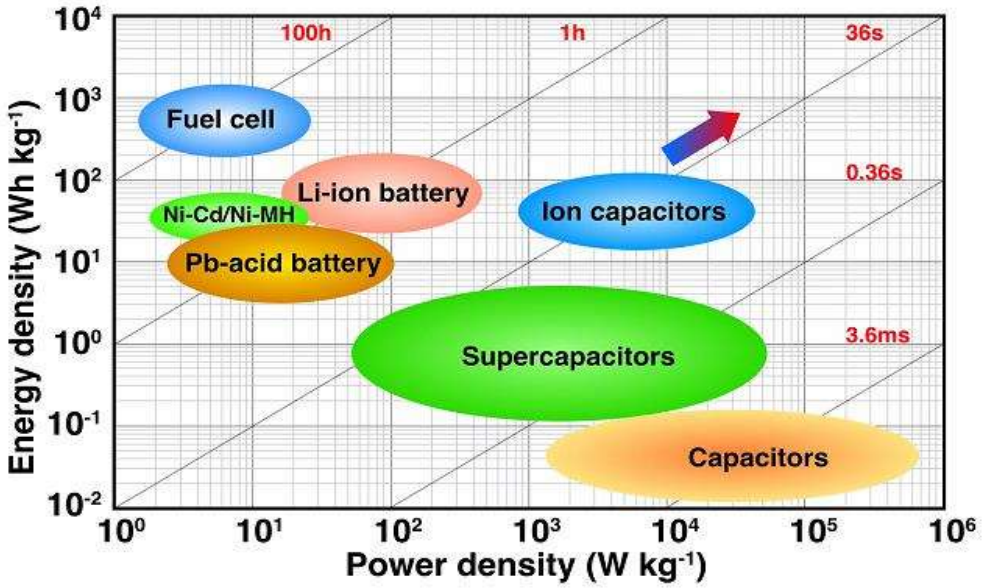

Figure 1.6: Rangone plot demonstrating energy and power relationship of different EES system [28]

Thus, batteries and supercapacitors have become the main EES technologies in today's market. Recently, several research efforts have been devoted to the advancements of metal-air batteries, Li/Na-ion batteries, and the pseudocapacitive electrodes enabled hybrid and asymmetric supercapacitors that can fulfil bulk energy storage and fast power requirements in the nearby future.

1.5.1 Historical perspectives

The exploration of electrochemistry and the emergence of electricity commenced during the late 18th century with Luigi Galvani's observation that a Frog's leg would twitch upon contact with a charged metal scalpel. This significant finding prompted Alessandro Volta to create the first battery, known as the Volta pile (Fig. 1.7). The Volta pile comprised alternating layers of copper and zinc disks, separated by cardboard saturated in salt water. This invention led to the revelation of water electrolysis and the formulation of different laws of electrochemistry.

Figure 1.7: Voltaic pile [29] (Figure is taken from open access internet source)

It is interesting to observe that the majority of battery technologies currently in use or under development were envisaged during the preceding two centuries., with the exception of the Li-ion battery.

Table 1.2 Development of various battery technologies [30]

Inventor	Technology	Year
A.Volta	First battery	1800
J. Frederic Daniell	Zn-Cu battery	1836
A.Smee	Metal-air battery	1840
G. Plante	Lead-acid battery	1859
G. Leclanche	Zn-MnO_2 battery	1868
T. deMichalowski	Ni-Zn battery	1899
W. Junger	Ni-Cd battery	1901
Multiple Inventor	Li-ion battery	1991

The first capacitor, named “Leyden jar” was invented by Ewald Georg von Kleist and Pieter van Musschenbroek in the middle of the eighteen century [31]. The modern theory of electrochemical double-layer capacitors (EDLC) emerged during the nineteenth by

interfacial electrochemists such as Gouy [32], Chapman[33], Stern [34], and Grahame [35]. In 1971, a new type of electrochemical capacitor called the pseudocapacitor was discovered, involving Faradaic processes, specifically in RuO_2 [36][37]. The discovery of pseudocapacitance introduced a new approach to boosting the energy density of electrochemical capacitors.

1.5.2 Electrostatic Capacitors

There are mainly three types of electrostatic capacitors, namely conventional capacitors, electrolytic capacitors, and ceramic capacitors. Conventional capacitors consist of two metal electrodes separated by a dielectric material, whereas, electrolytic capacitors utilize an electrolyte as a conductor between the dielectric and an electrode, and the thickness of the dielectric determines the working voltage of the capacitor. Ceramic capacitors, on the other hand, are fabricated by layering metal and ceramic materials, with the ceramic acting as the dielectric [38]. The amount of charge stored is determined by Eq. 1.1

$$Q = CV \dots\dots (1.1)$$

where Q represents the stored charge, V is the voltage between the plates, and C is the capacitance [39]. For an electrostatic capacitor, its capacitance is governed by Eq. 1.2

$$C = \varepsilon_0 \varepsilon_r \frac{A}{d} \dots\dots (1.2)$$

The total energy and maximum power stored in a capacitor are given by Eq. 1.3 and Eq. 1.4

$$E_{Total} = C \int_{V_{min}}^{V_{max}} V dV = \frac{1}{2} C V^2 \dots\dots (1.3)$$

$$P = IV = \frac{V^2}{4R_{cap}} \dots\dots (1.4)$$

These equations are also applicable to electrochemical double-layer capacitors, indicating the performance of capacitors can be enhanced by either expanding the operating potential window or reducing the internal resistance of capacitors.

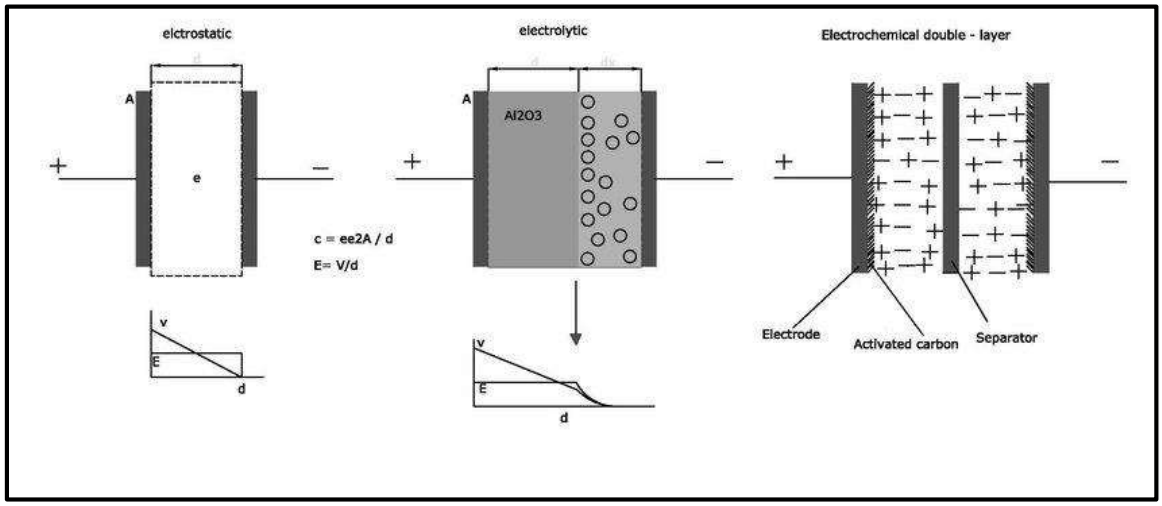

Figure 1.8: Schematic presentation of the electrostatic capacitor, electrolytic capacitor, and electrical double layer capacitor [38].

1.5.3 Batteries

A battery is a device that stores energy through the formation of chemical bonds and can be converted into electrical energy by means of an electrochemical redox reaction. In this device, the total energy stored (G) is an integral function of the overall capacity (Q) and the voltage (V):

$$G = \int Q\, dV \ldots\ldots (1.5)$$

The correlation between capacity and voltage varies significantly across different battery materials due to the inherent dissimilarity in the faradaic reaction. This reaction frequently leads to a phase alteration whenever an electrode material undergoes oxidation or reduction.

$$Q + ne \leftrightarrow R \ldots\ldots (1.6)$$

For an ideal battery with an invariant potential, the total stored energy can be expressed as:

$$G = QE \ldots\ldots (1.7)$$

The theoretical capacity of a battery can be determined by knowing the redox reaction taking place and by using Faraday's laws of electrolysis, which state that:

$$Q = \frac{nF}{M} \ldots\ldots (1.8)$$

Where F is the Faraday constant (96485 C mol^{-1}), n is the number of electrons transferred, and M is the molar mass of the material. The potential of a battery material is directly related to the change in the Gibbs free energy (ΔG) of the reaction and thus chemical potential (Δμ) upon reduction [40]:

$$E^0 = -\frac{\Delta G}{nF} = -\frac{\Delta \mu}{nF} \ldots\ldots (1.9)$$

This relationship forms the basis of the Nernst equation, which also accounts for the different activities of the materials involved in the redox reaction.

Further, batteries can be roughly divided into two categories namely; primary and secondary batteries. A primary battery is designed for single use only and discarded once it is depleted. On the other hand, a secondary battery (SB), also known as a rechargeable battery, is a type of battery that can be recharged multiple times before it needs to be rejected. Common examples of secondary batteries include lithium-ion batteries, nickel-cadmium batteries, and lead-acid batteries.

1.5.4 Types of rechargeable energy storage technologies

Based on their chemistry and configuration, secondary batteries can be classified into two groups: aqueous electrolytes-based and non-aqueous electrolytes-based SBs. Aqueous electrolyte-based (SBs) consist of lead-acid batteries, nickel-cadmium (Ni-Cd) batteries, nickel-metal hydride (Ni-MH) batteries, flow batteries, and metal-air batteries. On the other hand, non-aqueous electrolyte-based (SBs) include lithium-ion (Li-Ion) batteries, lithium polymer batteries, and sodium-ion (Na-ion) batteries.

1.5.4.1 Lead-acid batteries

Lead-acid batteries consist of two lead plates immersed in a sulphuric acid electrolyte solution. One plate is coated with lead dioxide (PbO_2), acting as a cathode, while the other plate is made of pure lead (Pb), acting as anode [41][42]. Lead-acid batteries have a high energy density and exceptional recyclability, with a recycling rate surpassing 99%. Despite these

advantages, Lead-acid batteries contain toxic lead and sulphuric acid, which can lead to soil and water contamination, posing risks to human health and the ecosystem [43].

During the charging/discharging process following reaction takes place:

$$PbSO_4(s) + H^+(aq) + 2e^- \leftrightarrow Pb(s) + HSO_4^-(aq)$$

$$PbSO_4(s) + 2H_2O(aq) \leftrightarrow PbO_2(s) + HSO_4^-(aq) + 3H^+(aq) + 2e^-$$

$$2PbSO_4(s) + 2H_2O(aq) \leftrightarrow Pb(s) + PbO_2(s) + 2HSO_4^-(aq) + 2H^+(aq) \quad E^0 = 2.048\,V$$

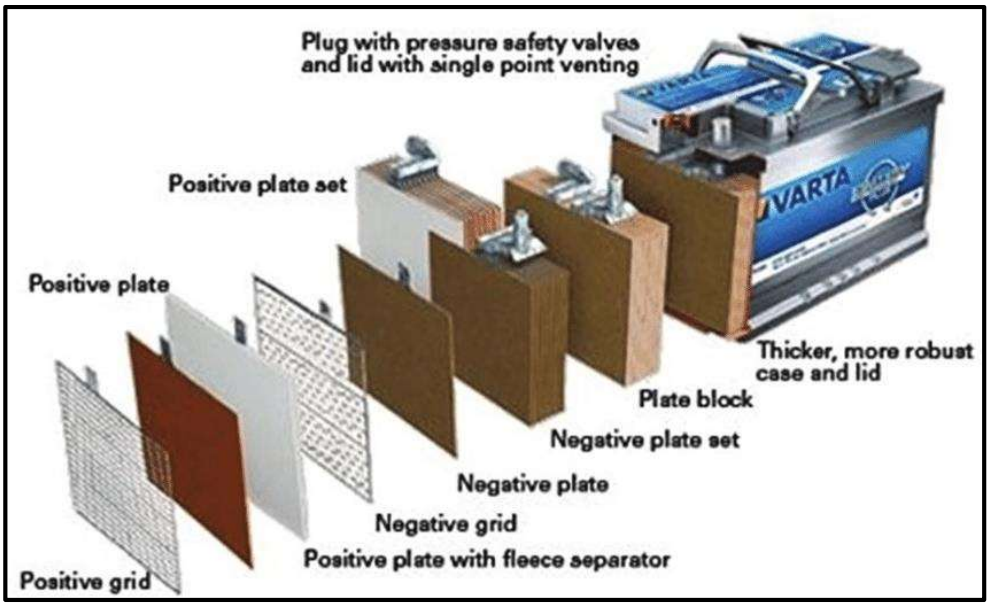

Figure 1.9: Lead-acid battery (Figure is taken from open access internet source) [41].

1.5.4.2 Nickel-cadmium (Ni-Cd) batteries

The Ni-Cd battery [44] has a positive electrode of nickel hydroxide and a negative electrode of cadmium compound. Potassium hydroxide is used as the electrolyte. During charge and discharge, the following reactions take place:

$$NiOOH(s) + H_2O(aq) + e^- \leftrightarrow Ni(OH)_2 + OH^-(aq)$$

$$Cd(s) + 2OH^-(aq) \leftrightarrow Cd(OH)_2 + 2e^-$$

$$2NiOOH(s) + Cd(s) + 2H_2O(aq) \leftrightarrow 2Ni(OH)_2 + Cd(OH)_2 \ldots\ldots\ldots E^0 = 1.32\,V$$

The water molecules, which are generated during charging, are consumed during discharging. Therefore, variations in electrolyte concentration are insignificant [45]. Further, cadmium, one of the key components, is toxic and need to be disposed properly.

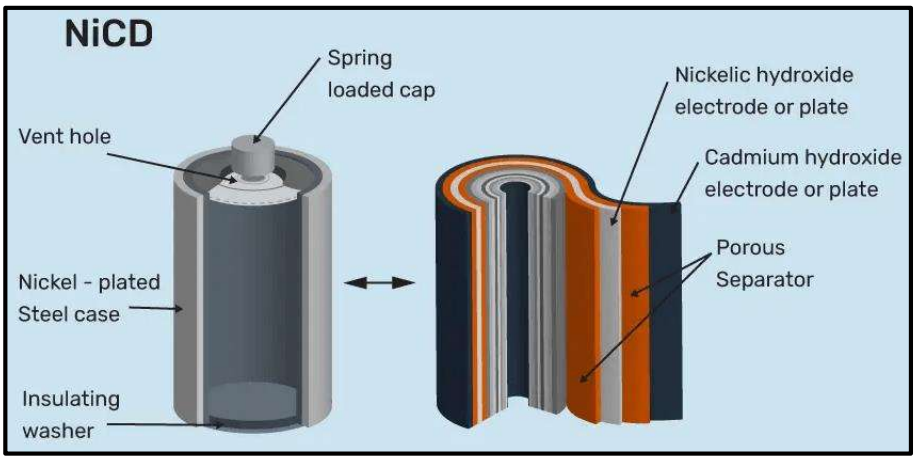

Figure 1.10: Ni-Cd battery (Figure is taken from open access internet sources) [44].

1.5.4.3 Nickel-metal hydride (Ni-MH) batteries

Nickel–MH batteries contain a nickel electrode as the positive electrode, and a hydrogen-absorbing alloy for the negative electrode. In the electrode reaction, the alloy electro-chemically absorbs and desorbs hydrogen in an alkaline solution (electrochemical reaction):

$$NiOOH(s) + H_2O(aq) + e^- \leftrightarrow Ni(OH)_2 + OH^-(aq)$$

$$MH(s) + OH^-(aq) \leftrightarrow M + H_2O + e^-$$

$$NiOOH(s) + MH(s) \leftrightarrow 2Ni(OH)_2 + M \dots\dots\dots E^0 = 1.32\,V$$

where M = hydrogen-absorbing alloy and MH = metal hydride.

In Nickel–MH batteries, the active material of the electrode reaction is hydrogen, and the hydrogen-absorbing alloy acts as a charge storing sites [46]–[48]. The capacity of the nickel–MH battery is approximately twice that of a standard Ni-Cd battery.

1.5.4.4 Metal-air batteries

Metal-air batteries consist of a metal anode, an air-breathing cathode, and an appropriate electrolyte. The metal anode can be alkali metals (such as Li, Na, and K), alkaline earth metals (like Mg), or first-row transition metals (such as Fe and Zn) with good electrochemical properties. The choice of the electrolyte, whether aqueous or non-aqueous, depends on the specific type of anode material used. The air-breathing cathode possesses a porous structure that facilitates continuous oxygen supply from the surrounding air [49]–[53].

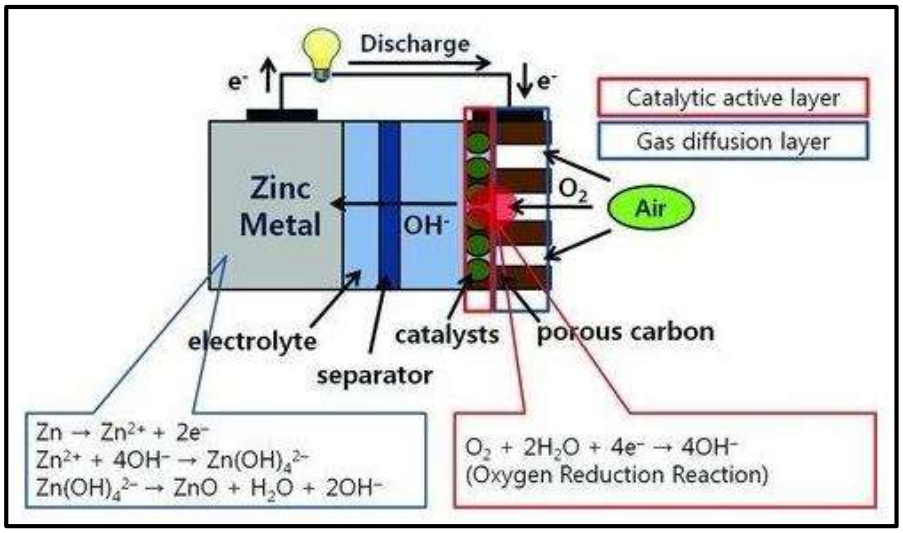

Figure 1.11: Schematic diagram of working principle of Zn-air battery [54].

During discharging, metal atoms at the anode react with the electrolyte to form metal ions and releases electrons. These metal ions then migrate through the electrolyte toward the cathode. At the cathode, oxygen from the air combines with water and the electrons received from the anode to form hydroxide ions. These hydroxide ions then react with the metal ions coming from the anode to reform the metal and regenerate the electrolyte, completing the electrochemical cycle.

In Aqueous electrolyte

$$\textbf{Anode:} \quad M \leftrightarrow M^{n+} + ne^{-}$$

$$\textbf{Cathode:} \quad O_2 + 2H_2O + 4e^{-} \leftrightarrow 4OH^{-}$$

In Non-aqueous electrolyte

Anode: $Li \leftrightarrow Li^+ + e^-$

Cathode: $O_2 + e^- \leftrightarrow O^{2-}$

$O^{2-} + Li^+ \leftrightarrow LiO_2$

$LiO_2 + Li^+ + e^- \leftrightarrow Li_2O_2$

Overall reaction: $O_2 + 2Li \leftrightarrow Li_2O_2$

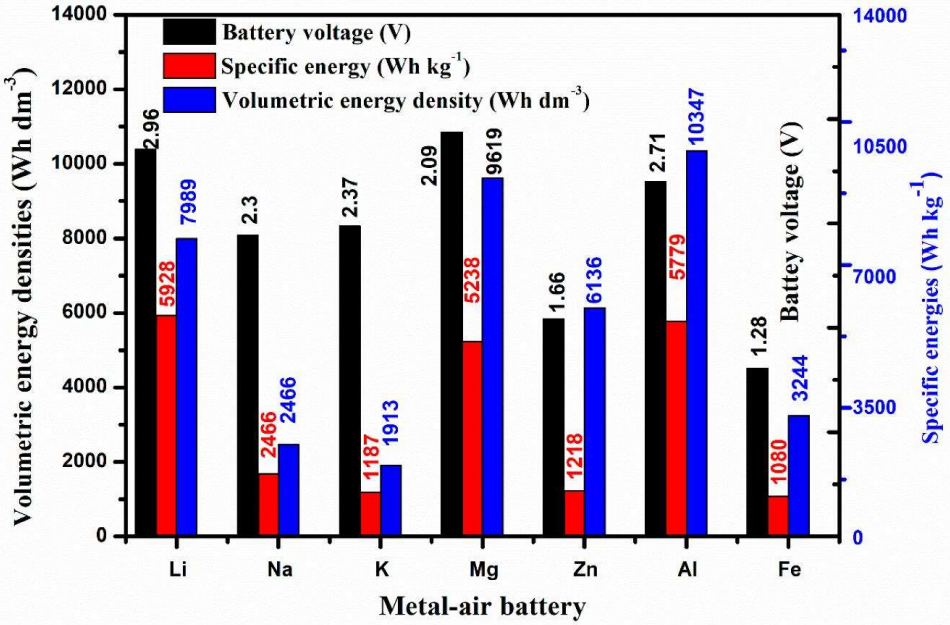

Figure 1.12: Theoretical energy density, specific energy, and nominal cell voltage of different types of metal-air batteries[55].

The Zn-air battery, introduced by L. Maiche in 1878, marked the beginning of metal-air batteries [53]. Since then, numerous metal-air battery variations have been consistently advancing, with the most recent innovations being the Zn-O_2 and Li-O_2 batteries [56][57].

1.5.4.5 Air Cathode and Role of OER and ORR Catalyst

Air cathode-supported OER/ORR catalyst plays a vital role in enhancing the performance, efficiency, and durability of metal-air batteries. During discharging, the cathode-supported catalyst facilitates the reduction of oxygen molecules (O_2) to form hydroxide ions (OH^-) by accepting electrons from the external circuit [58].

Oxygen Reduction Reaction (ORR): $O_2 + 2H_2O + 4e^- \leftrightarrow 4OH^-$

Subsequently, the generated OH^- will migrate toward the metal anode for the oxidation process. Hence, a cathode-supported ORR catalyst can provide the necessary electrons for the oxidation of hydroxide ions during the OER, maintaining a balanced charge transfer between the cathode and anode [59]. This improves the overall efficiency and stability of the battery.

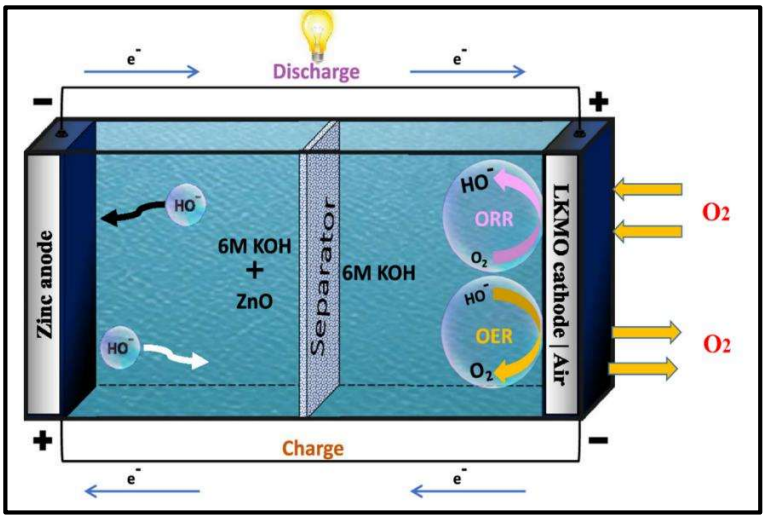

Figure 1.13: Schematic diagram of of Zn-air battery [60].

Oxygen Evolution Reaction (OER): $4OH^- \leftrightarrow O_2 + 2H_2O + 4e^-$

Currently, the performance of rechargeable metal-air batteries is hindered by sluggish reaction rate of OER/ORR occurring at the air cathode. So, understanding the reaction mechanism is important to develop an efficient OER/ORR catalyst [60][61].

1.5.4.6 Lithium-ion (Li-Ion) batteries

The basic structure of a lithium-ion battery is depicted in Fig. 1.14 [62]. Typically, the cathode material used is $LiCoO_2$, while the anode consists of graphite. The utilization of these electrode materials offers a high cell voltage of 3.6 V and an energy density of 120-150 Wh kg^{-1} [63]. The electrolyte employed is $LiPF_6$ dissolved in a mixture of organic solvents like ethylene carbonate and dimethyl carbonate. During the charging/discharging, the following reactions occur for energy storage.

Cathode: $LiCoO_2 \leftrightarrow Li_{1-x}CoO_2 + xLi^+ + xe^-$

Anode: $C_6 + Li^+ + e^- \leftrightarrow LiC_6$

Intercalation reactions can lead to a significant level of reversibility and commercial lithium-ion batteries can be rated approximately 500 charge/discharge cycles [64]. Additionally, the energy density of the cathode material can be improved by increasing the voltage from 3.6-3.9 V. Several higher voltage cathodes, such as the spinel $Li_yM_xMn_{2-x}O_4$ (where M = Cr, Fe, Co, Ni, and Cu) [65], have been proposed to address this issue, enabling energy storage between 4 and 5 V. However, pursuing the higher voltage required appropriate electrolytes selection, which is suitable for a 5 V potential range.

1.5.4.7 Challenges and shortcomings of Li-ion batteries

Despite their technological promise, Li-ion batteries still suffer from various drawbacks, especially in terms of safety. Li-ion batteries have a tendency to overheat and become damaged when exposed to high voltages. This can sometimes lead to thermal runaway and combustion [66]. Additionally, these batteries are prone to aging, resulting in capacity loss and frequent failures after a few years of use. Moreover, their adoption is hindered by their relatively high cost, which is approximately 40% higher. Furthermore, they are not optimal for applications that necessitate rapid charge storage, like regenerative braking [67].

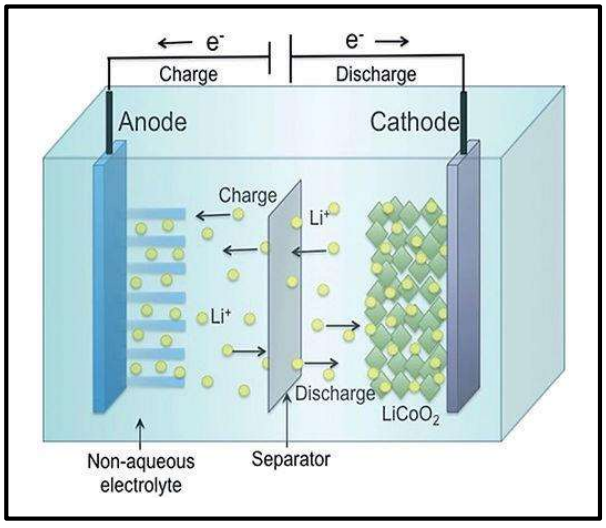

Figure 1.14: Basic configuration of a Li-Ion battery [62].

Although significant efforts have been made during the past decades to improve battery performance the main problem comes from peak usage. Even small electronic devices like mobile phones and laptops experience battery damage when their energy is suddenly drained. This problem is particularly pronounced in electric vehicles (EVs), where various factors such as driving style and road conditions lead to rapid fluctuations in power consumption and the battery pack fails to discharge quickly. Similarly, high currents generated during EV braking can have adverse effects on the battery's electrolytes. Consequently, there is an urgent need for an alternative solution that addresses the issues of short battery lifespan and insufficient power [68]. In the current scenario, a device with special capabilities like high power, energy density, and long cycle life is required. Modern high-power equipment demands large quantities of energy delivered rapidly, which conventional batteries and capacitors are unable to meet [69]. As a result, supercapacitors have emerged in recent decades as a viable solution, which fill the gap between batteries and capacitors.

1.5.5 Supercapacitor

Supercapacitors, also known as ultracapacitors, are emerging energy storage devices that provide a balanced combination of power and energy performance. They offer several advantages, including long cyclic life and the ability to charge and discharge rapidly, which make them suitable for high power applications. Currently, supercapacitors are used in conjunction with batteries for electric vehicles, which have been shown to reduce the overall size of the source, improve lifetime and reduce the energy loss of batteries [70]. Unlike ordinary capacitors, supercapacitors utilize electrostatic double-layer capacitance and electrochemical pseudocapacitance, both contributing to the total capacitance of the device, with a few differences. ESs can be classified into two categories based on the charge storage mechanism [71]: (i) electrochemical double-layer capacitors (EDLCs) and (ii) pseudocapacitors.

1.5.5.1 Electrochemical double-layer Capacitors (EDLC)

In EDLCs, the capacitance originated due to the accumulation of charges at the electrode/electrolyte interface, as depicted in Figure 1.15. The resulting capacitance is referred to as double-layer capacitance (C_{dl}) [72]. EDLCs, similar to traditional capacitors, comprise positive and negative electrodes submerged in an electrolyte. However, they

achieve a greater capacitance per unit volume by utilizing porous carbon materials with a high surface area as active components.

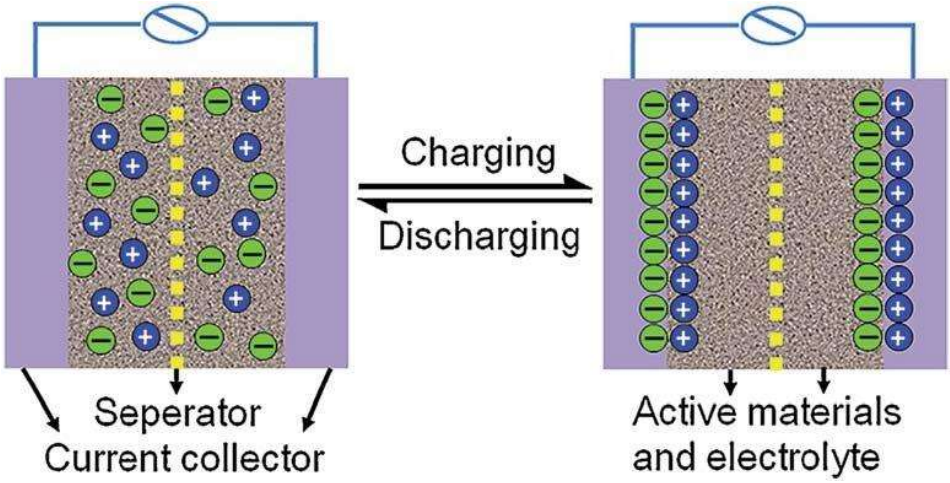

Figure 1.15: The charge storage mechanism of EDLC [73]

1.5.5.2 Principle of Charge Storage in EDLC

In order to understand the mechanism of charge storage, it is necessary to examine the origins and models of the double layer. Figure 1.16 illustrates a schematic representation of the Helmholtz model, Gouy-Chapman model, and Stern model [74]. The Stern model provides a more comprehensive understanding of the double-layer phenomenon compared to the Helmholtz and Gouy-Chapman models. Eq.1.10 relates the double layer C_{dl} of the electrode with Helmholtz (C_H) and diffuse layer (C_{diff}) contributions and the corresponding the equivalent circuit diagram has been shown below:

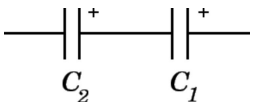

$$\frac{1}{C_{dl}} = \frac{1}{C_H} + \frac{1}{C_{diff}} \ldots\ldots (1.10)$$

Grahame modified the Stern model, by considering additional factors such as ionic radii and polarizability of cations and anions in electrolytes [74]. One significant aspect of the Grahame model is the distinction in the distances of the closest approach for cations and anions to the electrode surface. Due to the solvation shell around cations, they are located further away

from the electrode surface compared to anions [75]. This disparity in distance leads to the breakdown of the Helmholtz layer into inner and outer Helmholtz layers shown in Fig 1.17. Therefore, Eq.1.10 can be rewritten as Eq.1.11, to account for the capacitance contribution from the inner (C_{IH}) and outer (C_{OH}) Helmholtz layers.

$$\frac{1}{C_{dl}} = \frac{1}{C_{IH}} + \frac{1}{C_{OH}} + \frac{1}{C_{diff}} \dots\dots (1.11)$$

Previous studies have shown that porous carbon-based electrodes display a capacitance value (C_{dl}) of 15 to 50 μF cm^{-2} in aqueous electrolytes [76]. Assuming an average C_{dl} of 30 μF cm^{-2} and a surface area of 1000 m^2/g, the theoretical capacitance of such carbon material amounts to 300 F/g [77]–[79]. EDLCs function purely based on electrostatic principles without involving phase change, granting them exceptionally long cyclic life. Aqueous EDLCs have an operating voltage window of approximately 1.4 V to prevent water molecule decomposition, while EDLCs with organic electrolytes can operate within the range of 3.5 to 4 V [76]. Although, EDLCs with organic electrolytes give higher energy density, the electrolyte resistance reduces the power performance of the device [76].

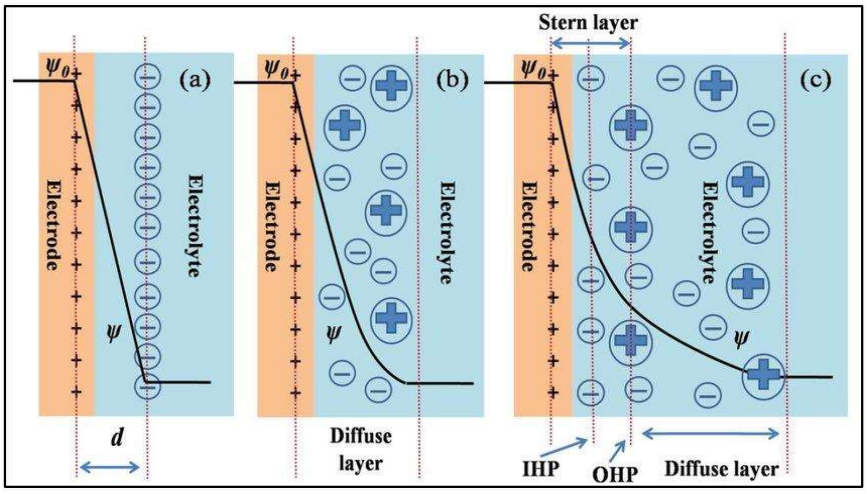

Figure 1.16: (a) Helmholtz model, (b) Gouy-Chapman model, and (c) Stern Model [74]

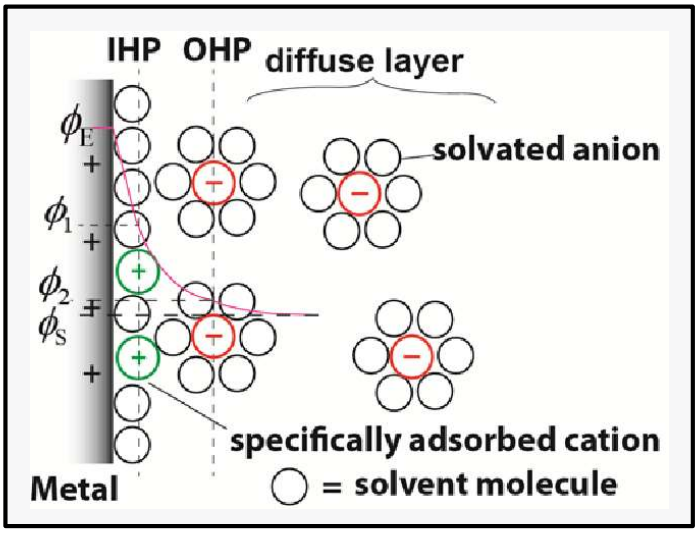

Figure 1.17: Schematic representation of Grahame Model [75].

1.5.5.3 Pseudocapacitors

Pseudocapacitors store energy through rapid and reversible redox reactions occurring at the electrode surface. Unlike EDLCs, pseudocapacitors provide capacitance that is 10 to 100 times higher due to charge storage not being restricted solely to the surface, but also extending to the nearby region where ion diffusion takes place [37]. Nevertheless, the slower faradic process hampers the power performance of pseudocapacitors when compared to EDLCs. In pseudocapacitance, the electrode's potential depends logarithmically on the extent of reactions. Conway has identified three faradic systems capable of generating pseudocapacitance: (a) underpotential deposition system, (b) redox pseudocapacitance, and (c) intercalation pseudocapacitance [80].

1.5.5.4 Principle of Charge Storage in Pseudocapacitors

From the thermodynamic point of view, pseudocapacitance can be related to potential by Eq.1.12, where α represents a system property that is directly proportional to the quantity of charge transferred [81].

$$\frac{\alpha}{1-\alpha} = Ke^{\frac{VF}{RT}} \dots\dots (1.12)$$

The storage of charge in the under-potential deposition system occurs through the potential-dependent adsorption of ad-atoms (H, Pb, Cu) onto the surface of the metal (Pt, Au, Ag). In the case of the H-Pt system, the process involves 2-dimensional surface reactions, which follows the Langmuir isotherm and Equation 1.12 can be rewritten as Equation 1.13

$$\frac{\Theta_H}{1-\Theta_H} = KC_{H+}e^{\frac{VF}{RT}} \dots\dots (1.13)$$

where θ_H represents the fractional surface coverage of H on Pt, and C_{H+} denotes the concentration of H^+ ions. This equation indicates a range of potential that corresponds to a range of θ_H. The definition of capacitance can be expressed using Equation 1.14.

$$C_\phi = \frac{nF}{RT}\left(\frac{X}{E}\right) \dots\dots (1.14)$$

$$C_\phi = q_H \frac{d\Theta_H}{dV} = \frac{q_H F}{RT}\Theta_H(1-\Theta_H) \dots\dots (1.15)$$

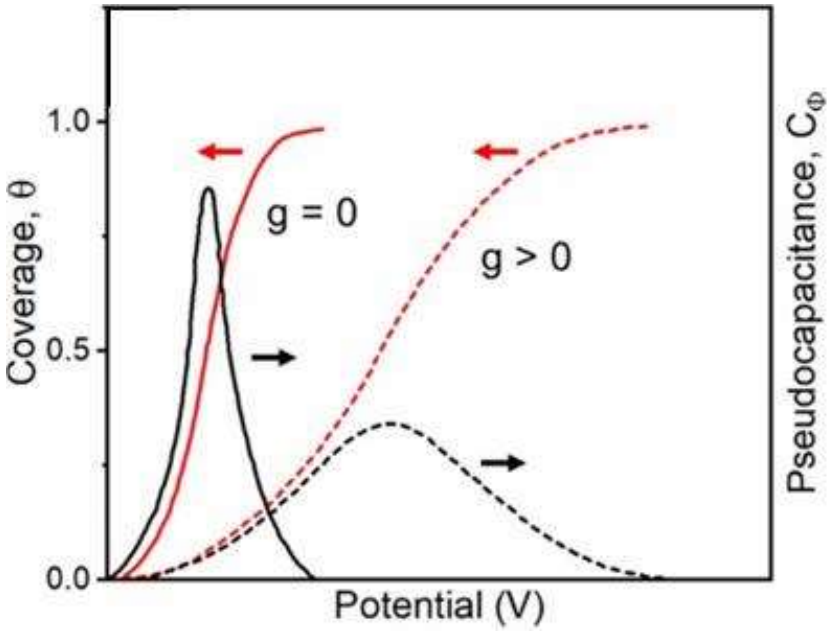

Figure 1.18: shows the variation of pseudocapacitance, Cφ, and surface coverage, Θ, for ideal Langmuir electrosorption (g=0) and Frumkin electrosorption (g>0) [74][82].

Based on Eq.1.15, the maximum capacitance can be obtained when $\theta_H = 0.5$. However, this capacitance calculation was based on the Langmuir isotherm, assuming no interactions between ad-atoms and metals. It is important to note that Boudart chemisorption often causes a change in surface electron distribution [74][82]. Consequently, Conway and Gileadi introduced an adsorption isotherm with an interaction energy term $g\theta$ to account for these interactions. Therefore, Eq.1.15 can be modified to Eq.1.16

$$C_\phi = \frac{q_H F}{RT} \frac{\Theta_H(1-\Theta_H)}{1+g\theta\,\Theta_H(1-\Theta_H)} \dots\dots (1.16)$$

Despite the significant pseudocapacitance resulting from underpotential deposition, the high cost of noble metal substrates has limited their applications.

In redox pseudocapacitance, the adsorption of ions is achieved by the charge compensation through redox reactions. Metal oxides and conducting polymers are examples of redox pseudocapacitive materials [76][83]–[85]. The redox reaction is expressed by the general chemical equation denoted as:

$$Ox + ne^- \rightarrow Red$$

For such a system, the Nernst equation can be applied which is given as:

$$E = E^0 + \frac{RT}{nF} \ln \frac{[Ox]}{[Ox]+[Red]} \dots\dots (1.17)$$

By rearranging the Nernst equation, we obtain Eq.1.18, which has a similar form to Eq.1.13, but with the property of concern of the extent of redox reactions. Therefore, it can be concluded that in redox pseudocapacitance, the potentials follow logarithmical relation with the extent of redox reactions.

$$\frac{[Ox]}{[Ox]+[Red]} = e^{\frac{\Delta EnF}{RT}} \dots\dots (1.18)$$

The intercalation pseudocapacitance arises when ions intercalate into tunnels or layers of active materials accompanied by faradic charge transfer with no crystallographic phase change [86]–[88]. Similar to under-potential deposition and redox pseudocapacitance, the extent

of intercalation can be related to a range of potential by Eq.1.19, where X is the fraction of ion occupancy in lattices.

$$\frac{X}{1-X} = e^{\frac{\Delta EnF}{RT}} \dots\dots (1.19)$$

Costentin and Saveant conducted an electrochemical study to investigate the origin of pseudocapacitance using MnO_2 and hydrous RuO_2 electrodes. The active centers in these materials are situated near the surface of the metal oxides at a distance of $<<(2Dt)^{1/2}$, where D represents the diffusion coefficient for charge compensating ions, and t is the diffusion time (s) [89]. Such analyses have confirmed that the electrochemical response in these materials results from the development of an electric double layer (EDL) on the conductive surface or a combination of surface Faradaic and EDL processes.

1.5.5.5 Electrochemical features of pseudocapacitors

Cyclic voltammetry is commonly used to study pseudocapacitance due to its ability to identify the "mirror image" criterion and the relationship between current and sweep rate. The pseudo linearity and hysteresis of galvanostatic discharge curves can also serve as indicators of pseudocapacitance. EIS offers the evaluation of pseudocapacitive behavior through analysis of real/imaginary impedance, real/imaginary capacitance, and phase angle. Fig. 1.19 presents cyclic voltammograms and galvanostatic discharge curves of representative materials. Within this classification, Type B pseudocapacitance is Faradaic in nature, while Type C Faradaic does not possess capacitive behavior.

1.6 Electrode Materials

Transition metal oxides and hydroxides are widely recognized as active materials for pseudocapacitors due to their variable stable oxidation states and high theoretical capacitances. These materials exhibit fast faradic reactions at their surfaces, resulting in higher energy densities compare to EDLCs. Numerous metal oxides and hydroxides, such as RuO_2, MnO_2, V_2O_5, NiO, Co_3O_4, Fe_2O_3, and FeOOH, have been extensively studied as active materials for energy storage systems (ESs). However, most of these metal oxides suffer from poor electrical conductivity and partial involvement in irreversible redox reactions.

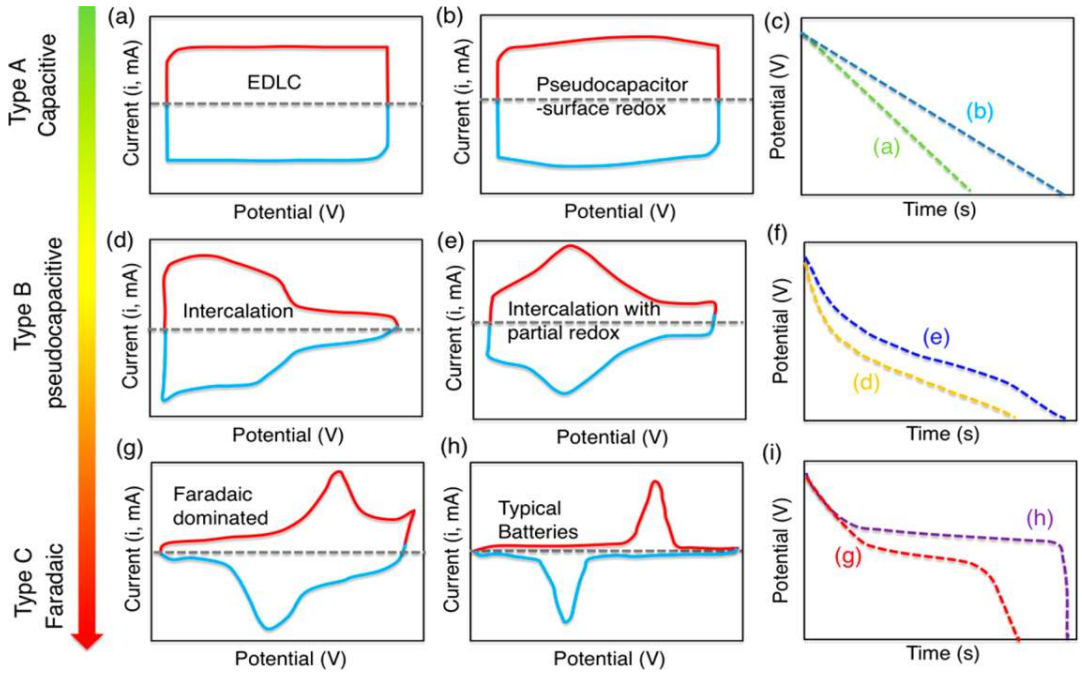

Figure 1.19: Schematic cyclic voltammograms (a,b,d,e,g,h) and corresponding galvanostatic profiles (c,f,i) of various types of charge storage systems [89].

To address this issue, conductive carbon materials are incorporated into the fabrication process to create composite materials [71], [90]. A brief review of different types of electrodes developed till now is presented below:

1.6.1 RuO_2

In 1971, Trasatti et al. successfully produced a thin film of RuO_2 through thermal decomposition, which demonstrated capacitive behavior when immersed in a 1M $HClO_4$ electrolyte within the voltage range of 0 to 1.45V vs. RHE [36]. Under acidic conditions, the charge storage mechanism of RuO_2 can be described as:

$$RuO_2 + xH^+ + xe^- \leftrightarrow RuO_{2-}(OH)_x$$

The pseudocapacitance observed in a thin film of RuO_2 can be attributed to the redox transition from Ru^{2+} to Ru^{4+} and the conversion of OH^- to O^{2-} within the structure [90]. The performance of RuO_2 electrodes is determined by charge transfer and diffusion processes within and between RuO_2 particles [91]. Between the two forms of RuO_2, the hydrous form

exhibits higher capacitance (342 F g^{-1}) compared to the anhydrous form (24 F g^{-1}). This difference can be explained using tree root model: anhydrous RuO_2 particles tend to agglomerate, resulting in limited micropores for ion diffusion, whereas hydrous RuO_2 particles are smaller and contain hydrated micropores that facilitate ion transport path [92].

Despite possessing the desired characteristics for applications in energy storage systems (ESs), the utilization of RuO_2 has been hindered by its high cost. To address this issue, researchers have explored alternative approaches such as creating RuO_2 composites using inexpensive metal oxides or depositing RuO_2 onto conductive substrates [93]. Hu et al. have synthesized a hydrous RuO_2-TiO_2 nanocomposite through a hydrothermal process, demonstrating exceptional capacitance of 992 F g^{-1} at a scan rate of 100 mV s^{-1} [94]. In another investigation, Hsieh et al. formed a composite by coating vertically aligned MWCNTs with hydrous RuO_2 on a titanium current collector, resulting in a maximum capacitance of 1652 F g^{-1} [95] was achieved.

1.6.2 MnO_2

Extensive research has been conducted on MnO_2 for its application in ESs, because of its high theoretical capacitance of 1370 F g^{-1}, low-cost, low toxicity, and the availability of multiple oxidation states [96]. Similar to RuO_2, the pseudocapacitance of MnO_2 is attributed to the successive redox transitions of Mn^{3+} and Mn^{4+}, as described as:

$$MnO_2 + C^+ + e^- \leftrightarrow MnOOC$$

One advantage of MnO_2 over RuO_2 is its ability to operate in a mild aqueous electrolyte such as Na_2SO_4 and chloride salts (KCl, NaCl), unlike the strong acid or base electrolytes required by RuO_2 systems [90]. MnO_2 have several polymorphs, namely α, β, γ, δ, and λ phases and play a crucial role in determining its electrochemical performance. Each phase possesses distinct charge storage sites for electrolyte accumulation. Brousse et al. and Devaraj et al. conducted studies to measure the capacitance of different MnO_2 structures in 0.1M K_2SO_4 and 0.1M Na_2SO_4 solutions, respectively. Both researchers observed that the capacitance of MnO_2 follows the order of $\alpha \cong \delta > \gamma > \lambda > \beta$ [97][98]. In another study, Ghodbane et al. establish a relationship between the surface area and capacitance of various MnO_2 structures. The study demonstrated that the capacitance of MnO_2 is strongly correlated with ionic

conductivities rather than the BET surface area [99]. These findings indicate that the charge storage mechanism of MnO_2 involves not only surface reactions but also ion intercalation into the bulk MnO_2 [98][99]. Despite its high theoretical capacitance and compatibility with aqueous electrolytes, one of the major drawbacks of MnO_2 is its low electrical conductivity, which results in reduced capacitance and poor rate performance [93][96].

1.6.3 V_2O_5

V_2O_5 has demonstrated impressive performance as the electrode material, which exhibited high energy density, low toxicity, a stable layered structure, and a wide potential window resulting from various oxidation states ranging from V^{2+} to V^{5+} [71][91][100]. Lee and Goodenough synthesized composite of amorphous V_2O_5 .nH_2O and made deposited on titanium substrate [101]. The fabricated electrode exhibited high specific capacitance of 346.4 F g^{-1} with a nearly symmetrical CV in voltage range of -0.2 to 0.8 V versus a saturated calomel electrode (SCE) in a 2M KCl electrolyte at pH= 2.32 [101]. However, they also found that the V_2O_5 composite electrode undergoes dissolution at -0.1 V versus SCE in a 2M KCl solution at pH = 6.67. They concluded that adjusting the electrolyte pH to a more acidic condition helps to mitigate the dissolution behavior of V_2O_5. In another experiment, Qu et al. employed a core-shell structure of polypyrrole (PPy) on V_2O_5 nanoribbons to decrease the dissolution and enhance conductivity and the fabricated electrode exhibited a high specific capacitance of 308 F g^{-1} in a 0.5 M K_2SO_4 electrolye [102]. Furthermore, the electrode was tested up to 10000 cycles and experienced a capacitance loss of less than 5%, whereas pure V_2O_5 exhibited a loss of 17.5% [102].

1.6.4 Nickel oxide (NiO) & nickel hydroxide ($Ni(OH)_2$)

NiO shows great potential for application in energy storage systems (ESs) due to its high theoretical capacitance of 2584 F g^{-1}, low cost, and non-toxicity [103][104]. The electrolyte used for the NiO electrode is usually alkaline, although the exact mechanism for charge storage is unclear. Two theories have been proposed for the pseudocapacitance of NiO, the first theory involves redox reactions between NiO and nickel oxyhydroxide (NiOOH), while the second theory suggests reactions between $Ni(OH)_2$ and NiOOH [93]. However, it is widely accepted that the occurrence of NiOOH is the initial step, followed by reversible redox reactions between $Ni(OH)_2$ and NiOOH [104].

$$NiO + OH^- \leftrightarrow NiOOH + e^-$$

$$NiO + H_2O + e^- \leftrightarrow NiOOH + H^+ + e^-$$

$$Ni(OH)_2 \leftrightarrow NiOOH + H^+ + e^-$$

$$Ni(OH)_2 + OH^- \leftrightarrow NiOOH + H_2O + e^-$$

$Ni(OH)_2$ exists in two polymorphs, namely α-$Ni(OH)_2$ and β-$Ni(OH)_2$ both having a hexagonal layered structure. α-$Ni(OH)_2$ has intercalated anions with the presence of water moieties, whereas water is absent in β-$Ni(OH)_2$ [105]. Consequently, α-$Ni(OH)_2$ demonstrates a higher specific capacitance than β-$Ni(OH)_2$. This can be explained by recalling that hydrous RuO_2 showed higher specific capacitance than the anhydrous form due to improved ion transport [92][106][107].

1.6.5 Cobalt oxide (Co_3O_4) & cobalt hydroxide ($Co(OH)_2$)

Co_3O_4 is another alternative active material for ESs application, which shows a high theoretical capacitance of 3560 F g^{-1}, low cost, good corrosion resistance, and high electrochemical stability [71][104]. Co_3O_4 can be operated in an alkaline medium, and the charge storage mechanism is represented as:

$$Co_3O_4 + H_2O + OH^- \leftrightarrow 3CoOOH + e^-$$

Salunkle et al. have synthesized nanoporous Co_3O_4 using a metal-organic framework, and the electrode exhibited a specific capacitance of 504 F g^{-1} at a scan rate of 5 mV s^{-1} in a 6M KOH electrolyte [108]. The cyclic stability was also tested and was found to be increased to 1100 F g^{-1} after 500 cycles [109]. The authors suggested that this phenomenon was attributed to the activation process, where the electrode access more ions during the charge-discharge process. The α-$Co(OH)_2$ showed specific capacitance of 735 F g^{-1} [110], while thin film of β-$Co(OH)_2$ exhibited specific capacitance of 890 F g^{-1} in 1M KOH electrolyte in the potential window of -0.2 to 0.4 V vs. SCE [111].

1.6.6 Iron oxide (Fe_2O_3) & iron hydroxide (FeOOH)

Iron oxides (Fe_2O_3 or Fe_3O_4) exhibited superior pseudocapacitive charge storage performance due to its fast reversible Fe^{2+}/Fe^{3+} redox reaction, large HER overpotential, low cost, and high theoretical capacitance. However, their inferior conductivity (~10-14 S cm^{-1})

and low ionic diffusion rate lead to the low power density. In order to overcome this issue, many iron oxides-based composite has been formed, which show high electrochemical active area and shorter ion diffusion length. Xia et al. prepared Fe_2O_3 quantum dot (QD = 2 nm) on functionalized graphene sheet, which showed superb specific capacitance of 347 F g^{-1} between -1-0 V (vs Ag/AgCl) in Na_2SO_4 electrolyte. The charge storage mechanism of Fe_2O_3 in an alkaline medium is given as following:

$$\frac{1}{2}Fe_2O_3 + \frac{3}{2}\,H_2O + e^- \leftrightarrow Fe(OH)_2 + OH^-$$

Liang and co-workers proposed a phosphine plasma activation method to enhance the capacitive performance of Fe_2O_3 nanorods [112]. The dense Fe_2O_3-P electrode produced a large areal capacitance of 340 mF cm^{-2}, which is much larger than that of pristine Fe_2O_3 with only 66 mF cm^{-2} within -0.8-0 V (vs Ag/AgCl) in 1M Na_2SO_4 electrolyte.

1.6.7 Intercalation Pseudocapacitance in Transition metal oxides

Layered transition metal oxides can efficiently store charge via intercalation/deintercalation of ions for high energy and power density applications. The wide interlayer spacing and weak interlayer bonding of layered oxide materials allows for the access of a large variety of guest species, including cations, anions, and polymers. Additionally, the ability to fine-tune the solid-state environment of layered oxides is highly beneficial, to allow multivalent ion intercalation, improved interfacial charge transfer and/or solid-state diffusion. Intercalation pseudocapacitance occurs due to redox reactions at the surface as well as the bulk that are not kinetically limited by solid-state diffusion or phase transitions. The general intercalation equation can be expressed as:

$$MA_y + xLi^+ + xe^- \leftrightarrow Li_xMA_y$$

The layered oxides are typically formed by transition metals in high oxidation states +4, +5, and +6. Here, some of the transition metal oxides which possess layered structures are given as followings:

1.6.7.1 TiO_2-(B)

The pseudocapacitive behavior of TiO_2-(B) was attributed to its open structure with ion intercalation channels parallel to the b-axis [113]. There is three different Li^+ sites in TiO_2-(B), namely, C, A2, and A1 (Fig. 1.20) which exhibit different site energies and diffusion barriers [114]. Hua et al. performed a comprehensive experimental study on the lithiation mechanism of TiO_2-(B) nanoparticles by combining in situ X-ray and galvanostatic intermittent titration technique (GITT) and concluded that materials structure and electrochemical properties are interconnected to each other in order to develop high power energy storage materials [115].

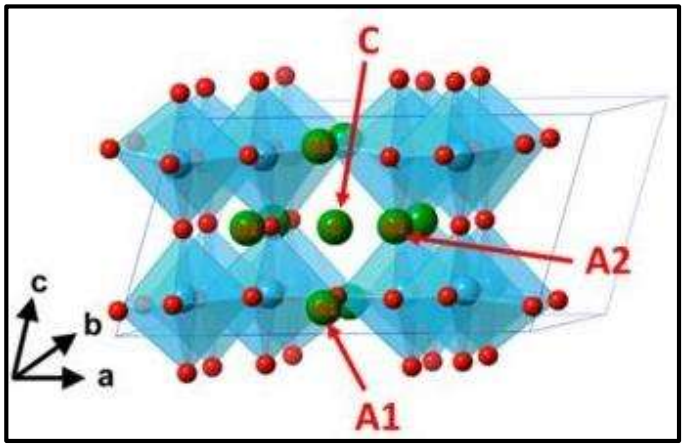

Figure 1.20: Li^+ insertion sites in TiO_2 nanoparticles [114].

1.6.7.2 T-Nb_2O_5

An analysis of the lithiation kinetics and the associated structural response of T-Nb_2O_5 was carried out by Augustyn et al [116]. CVs of T-Nb_2O_5 in 1 M $LiClO_4$ at rates between 0.1 to 500 mV/s, and logarithmic plotting of the peak current versus sweep rate revealed the presence of two kinetic regimes (Fig. 1.21 A, B): (i) fully surface-controlled kinetics up to 20 mV/s (b = 1) with no solid-state diffusion limitations, reaching a specific capacity of about 130 mAh/g within 60 s of charging; and (ii) mainly diffusion-controlled kinetics above 50 mV/s ($0.7 < b < 0.8$) [115]. In situ, XAS confirmed the continuous change in oxidation state from Nb^{5+} to Nb^{4+} (Fig. 1.21C), and EXAFS showed a two-stage intercalation process (Fig. 1.21D): first, various Nb−O bond lengths (1.40−1.80 Å) merged

to an intermediate bond length (1.75 Å), followed by an increase of Nb-O distances to 1.85 Å because of increased Li-O interaction with increasing lithiation of the structure [116]. This behavior underlined the need for an intercalation host with an open interconnected layered structure, which enable fast lithium diffusion with no phase transformation [116].

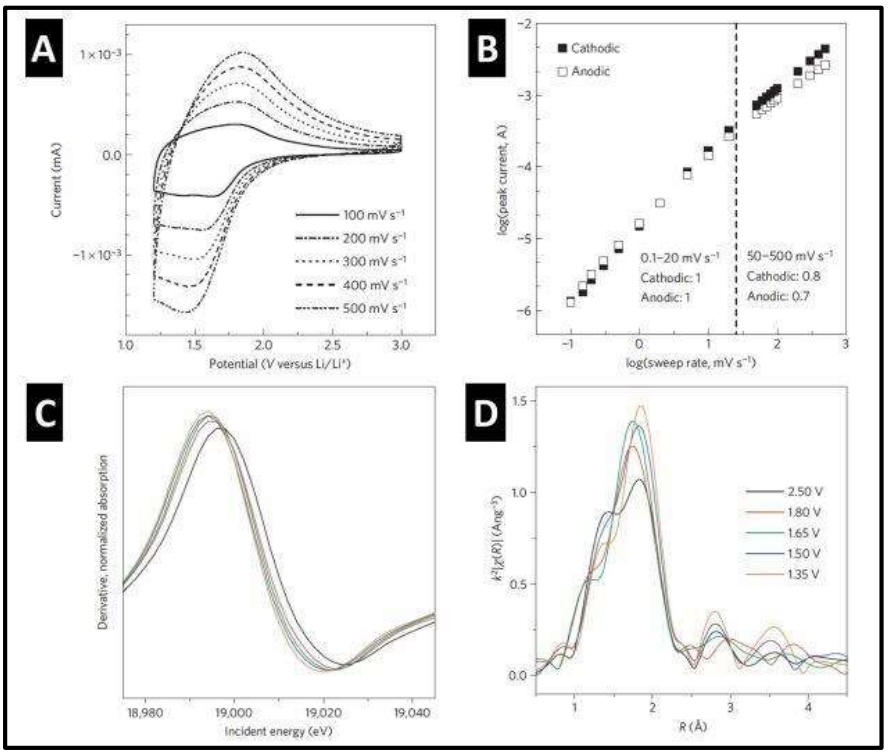

Figure 1.21: (A) CVs, (B) b-value determination, (C) derivative of Nb K-edge from in situ XAS, and (D) k^2-weight FT K-edge from EXAFS at specific potential vs Li/Li^+ [116].

1.6.7.3 Perovskite Oxides

Many perovskites possess a wide range of oxygen deficiencies and oxygen excess in which reversible charge storage takes place. For example, $LaMnO_{3+\delta}$ accommodates both sub- and super stoichiometric oxygen content, with $-0.25 < \delta < 0.25$ [117]. CV curves showed a rectangular shape with a small, reversible peak around −0.4 V vs Hg/HgO (Fig. 1.22). The proposed reaction mechanism was given as:

$$La\left[Mn^{2+}_{2\delta}; Mn^{3+}_{1-2\delta}\right]O_{3-\delta} + 2\delta\, OH^- \leftrightarrow LaMn^{3+}O_3 + 2\delta e^- + \delta H_2O$$

$$LaMn^{3+}O_3 + 2\delta\, OH^- \leftrightarrow La\left[Mn^{4+}_{2\delta}; Mn^{3+}_{1-2\delta}\right]O_{3+\delta} + 2\delta e^- + \delta H_2O$$

Liu et al. studied the electrochemical performance of $PrBaMn_2O_{6-\delta}$ (f-PBM) and reduced $PrBaMn_2O_{6-\delta}$ (r-PBM) and found that r-PBM with a single cubic phase exhibited metallic character in its ground state whereas f-PBM with hexagonal structure has a small band gap of 1.39 eV, exhibiting poor conductivity, as compared to cubic phase [118]. Using XANES, it was found that the introduction of oxygen vacancies in the structure led to partial oxidation of Mn^{2+} to Mn^{4+} (Fig. 1.22) and generate a pseudocapacitive response up to a scan rate of 20 mV/s. DFT calculations predicted that the layered double perovskite structure benefited both the oxygen vacancy concentration and O^{2-} diffusion rate, which could guide further materials design strategies for pseudocapacitive perovskite electrodes [116].

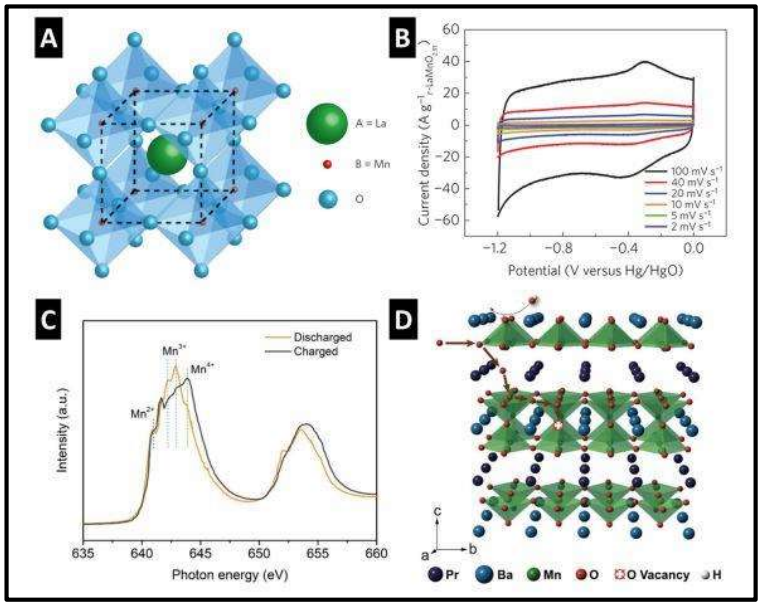

Figure 1.22: (A) Crystal structure of $LaMnO_3$, (B) CVs of $LaMnO_{2.91}$ in 1M KOH [117], (C) XANES of charged and discharged $PrBaMn_2O_{6-\delta}$, and (D) intercalation of O^{2-} in $PrBaMn_2O_{6-\delta}$ structure [118].

1.7 Electrochemical Devices

Supercapacitor device generally consist of one positive electrode (cathode), one negative electrode (anode) soaked in an electrolyte, separated by an ion-permeable membrane. Electrolytes may be aqueous or non-aqueous. Each electrolyte can be stably operated only within a certain potential range. Researchers are always trying to develop electrode materials that possess stable electrochemical performances in a separate potential window in order to construct high-voltage supercapacitor devices. The positive and negative

electrode materials have their own standard electrode potentials, which are related to their Fermi energies, $\mathcal{E}_F$, and decide the overall working potential window of the device [119]. Fig. 1.23, illustrates the standard electrode potential of some common widely used electrodes and their relationship with electrolyte.

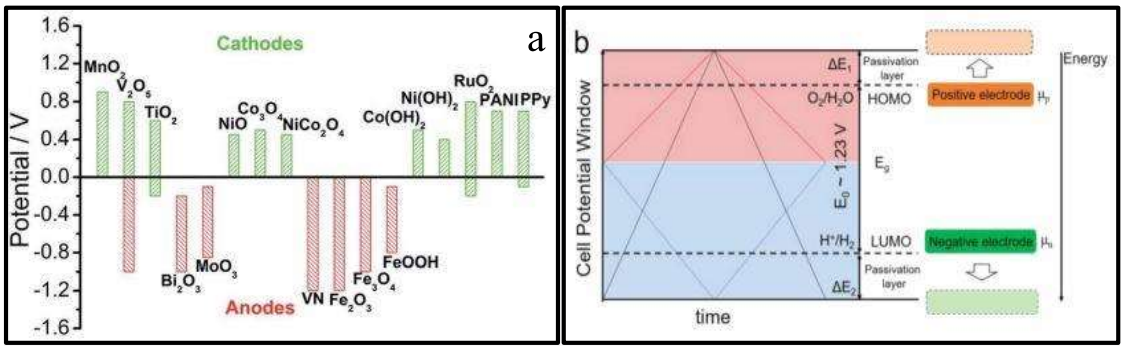

Figure 1.23: (a) standard electrode potential of some common widely used electrodes, and (b) cell voltage of an aqueous system along with electron energies of active materials [120].

The operating voltage of a supercapacitor is determined by three key factors: the stable potential window of the electrolyte, the standard potential range of each electrode, and the formation of passivation layer at the electrode/electrolyte interface. Theoretically, the potential window of the supercapacitor can be expressed as [121]:

$$E_{device} = E_{positive} - E_{negative} \dots\dots (1.20)$$

Whereas, depending upon the standard electrode potential of an electrode, the potential window of the supercapacitor can be evaluated from the following Eq. 1.21 [122]:

$$E_{device} = E_0 + \Delta E_1 + \Delta E_2 = \frac{(\omega^{\beta} - \omega^{\alpha})N_A}{F} + \Delta E_1 + \Delta E_2 \dots\dots (1.21)$$

where ΔE_1 and ΔE_2 are the working potential window of the positive electrode and negative electrode in three-electrode assembly, ω^{α} & ω^{β} is the work function of the positive and negative electrode, respectively. Over the past few decades, different types of devices have been envisaged to increase the energy density of SCs [123][124]. These devices can be categorized into four basic configurations: type I, which uses symmetric electrodes based on EDLC, type II, which utilizes symmetric electrodes based on pseudocapacitive electrodes,

type III, which combines EDLC and pseudocapacitive electrodes in an asymmetric configuration, and type IV, which consists of asymmetric electrodes using two different pseudocapacitive materials.

1.7.1 Symmetric Cell

Conventional symmetric supercapacitor device consists of electrodes with the same type of electrode materials and the same mass loading, and covers only a narrow potential range. For example, symmetric supercapacitors made of using graphene (EDLC type) as an electrode material showed a rectangular CV, whereas symmetric supercapacitor made of graphene oxide (pseudocapacitive type) exhibited a quasi-rectangular CV curve [125]. The basic electrochemical features of a symmetrical device are given as following:

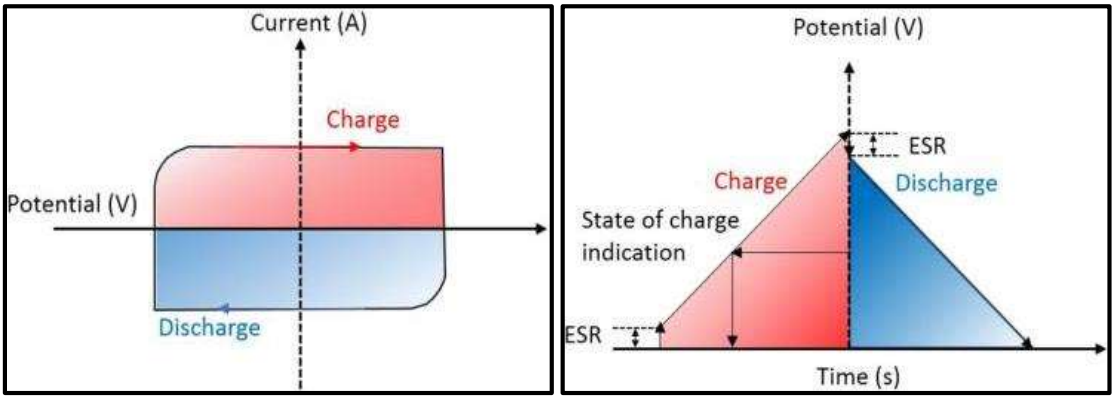

Figure 1.24: CV and GCD curves of symmetrical EDLC- types of electrodes.

1.7.2 Hybrid Cell

The hybrid capacitor describes the case where the two electrodes have two different charge-storage mechanisms: one capacitive and one battery-type Faradaic. For example, devices consisting of a Faradaic electrode ($Ni(OH)_2$) and a carbon electrode represent hybrid capacitor device [126]. Although one electrode performs as a battery electrode, the CV and GCD curves of the full device can exhibit more capacitive-like behavior rather than perfect ideal capacitive characteristics. The energy density of a hybrid capacitor, with a nonlinear GCD curve can be estimated by Eq. 1.22:

$$E = \int Q\, dV = \int_{t_1}^{t_2} IV_{(t)}\, dt \ldots\ldots (1.22)$$

Where, t_1 represents the time after initial iR drop, t_2 is the time at which discharged is finished, and I is the constant current applied to the supercapacitor.

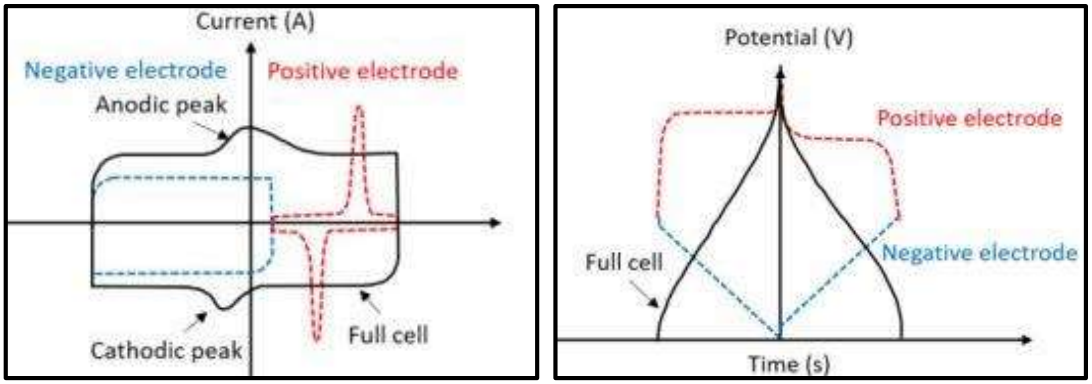

Figure 1.25: Schematic illustration of hybrid capacitor [126].

1.7.3 Asymmetric Cell

The purpose of making an asymmetric configuration is to increase the energy density of a supercapacitor device by extending the operational potential window. Tang et al. developed Fe_2O_3 nanowires and NiO nanoflakes on carbon fibre paper (CFP) as a negative and positive electrode respectively. The as-fabricated asymmetric device exhibited a high energy density of 105 Wh/kg at a power density of 1400 W/kg and still retains 72.6 Wh/kg at 12700 W/kg, which is superior to previously reported ASCs [120].

Thus, the concept of an asymmetric supercapacitor was considered as one way to solve the issues of the narrow potential window and the relatively low energy density of a supercapacitor device.

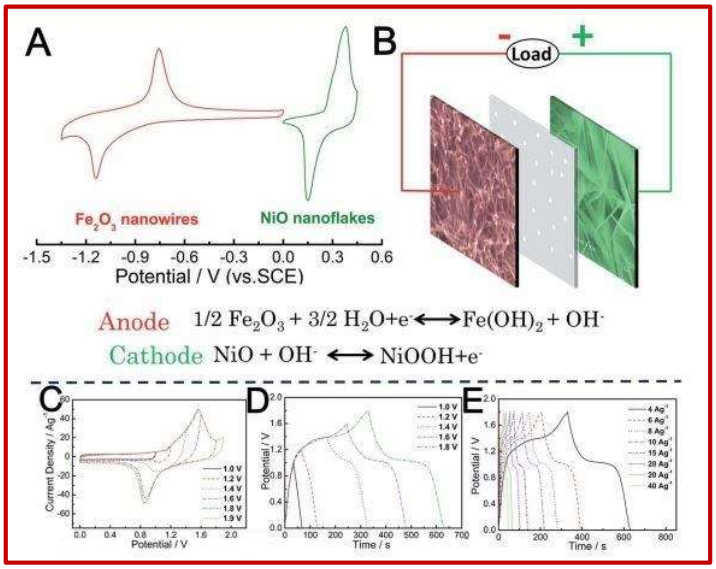

Figure 1.26: Electrochemical features of NiO ‖ Fe_2O_3 device in 6M KOH electrolyte [120]

1.8 Aim of the Thesis

The aim of this thesis is to provide a correlation between crystal structure and electronic properties of the materials, for developing high performing pseudocapacitor electrodes. Layered transition metal oxides having open channel structures are envisaged here as a promising candidate that enables fast diffusion of ions into the open framework and showed high energy density and power-delivering capabilities. The redox energy of the materials depends on their local electronic structure, via the formation of metal-ligand bonds. Hence, tailoring the crystal structure through suitable dopant concentration can significantly shift these energy bands and provide an opportunity to enlarge the operating potential window. Another aim of this thesis is to construct an aqueous-based asymmetric supercapacitor devices (ASCs), that comprise an optimized matching of electrode materials in combination with appropriate electrolytes and the current collector. Therefore, developing wide voltage aqueous ASCs can achieve the target of meeting high energy and power density, simultaneously. Furthermore, the present thesis emphasizes a better understanding of the kinetics of electrochemical reactions at the electrode/electrolyte interfaces, providing crucial information about cell design and development of bi-functional OER/ORR catalysts for grid-scale energy storage solution.